ACS Combinatorial Science

Research Article

pubs.acs.org/acscombsci

Mapping Quantum Yield for (Fe−Zn−Sn−Ti)O_x Photoabsorbers Using a High Throughput Photoelectrochemical Screening System

Chengxiang Xiang,*[,†] Joel Haber,[†] Martin Marcin,[†] Slobodan Mitrovic,[†] Jian Jin,[†,‡] and John M. Gregoire*[,†]

[†]Joint Center for Artificial Photosynthesis, California Institute of Technology, Pasadena, California 91125, United States

[‡]Engineering Division, Lawrence Berkeley National Laboratory, Berkeley, California 94720, United States

ABSTRACT: Combinatorial synthesis and screening of light absorbers are critical to material discoveries for photovoltaic and photoelectrochemical applications. One of the most effective ways to evaluate the energy-conversion properties of a semiconducting light absorber is to form an asymmetric junction and investigate the photogeneration, transport and recombination processes at the semiconductor interface. This standard photoelectrochemical measurement is readily made on a semiconductor sample with a back-side metallic contact (working electrode) and front-side solution contact. In a typical combinatorial material library, each sample shares a common back contact, requiring novel instrumentation to provide spatially resolved and thus sample-resolved measurements. We developed a multiplexing counter electrode with a thin layer assembly, in which a rectifying semiconductor/liquid junction was formed and the short-circuit photocurrent was measured under chopped illumination for each sample in a material library. The multiplexing counter electrode assembly demonstrated a photocurrent sensitivity of sub-10 μA cm^{-2} with an external quantum yield sensitivity of 0.5% for each semiconductor sample under a monochromatic ultraviolet illumination source. The combination of cell architecture and multiplexing allows high-throughput modes of operation, including both fast-serial and parallel measurements. To demonstrate the performance of the instrument, the external quantum yields of 1819 different compositions from a pseudoquaternary metal oxide library, (Fe−Zn−Sn−Ti)O_x, at 385 nm were collected in scanning serial mode with a throughput of as fast as 1 s per sample. Preliminary screening results identified a promising ternary composition region centered at $Fe_{0.894}Sn_{0.103}Ti_{0.0034}O_x$, with an external quantum yield of 6.7% at 385 nm.

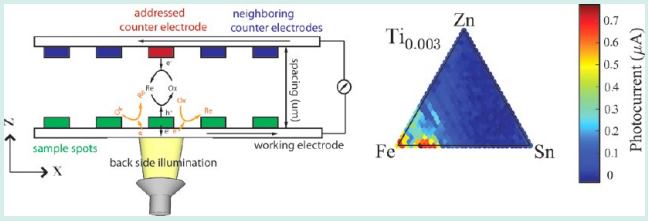

KEYWORDS: *photoelectrochemistry, metal oxides, semiconductor liquid junction, quantum yield*

INTRODUCTION

Light absorbers play a critical role in photovoltaic cells and photoelectrochemical cells, where the incident photons are absorbed and energetic electrons and holes are generated and transported either to provide current to an external circuit or to catalytic sites for efficient bond making and breaking.[1−3] To evaluate the performance of a light absorber, an asymmetric junction is typically introduced to measure the charge separation and voltage generation properties. These junctions could be homojunctions or heterojunctions, including semiconductor/metal Schottky junctions, semiconductor/liquid junctions, semiconductor/polymer junctions, etc.[2,4,5] Combinatorial synthesis and screening of light absorbers have received increasing attention due to the need for high performance material discovery. In the area of solar-to-fuel research and development, most studies have been carried out in an aqueous electrolyte to identify promising photocatalysts for a particular fuel forming reaction, such as the oxygen evolution reaction or the hydrogen evolution reaction.[6−12] In these studies, the carrier generation and transport through the semiconductor (photocatalyst) interface are governed not only by the fundamental energy conversion property of the semiconductor, interfacial energetics between the semiconductor and the fuel forming redox couple but also the kinetics of the electrocatalysis of the particular reaction. Thus, most reported measurements do not reflect the intrinsic semiconductor performance. For instance, one of the most common figures of merit in these measurements, the short-circuit photocurrent, could be obscured by poor electrocatalytic properties even if the semiconductor has good carrier collection efficiency.

Semiconductor/metal junctions were extensively studied even in some of the unconventional solar absorber materials, such as Cu_2O, Zn_3P_2, etc., in the 1980s.[13,14] However, combinatorial synthesis and evaluation of Schottky junctions have many challenges, including confounding interfacial solid state reactions, and have not been reported to date. Semiconductor/liquid junctions, more specifically semiconductors in contact with a one-electron reversible redox couple, such as a metallocene system, offer an alternative to solid state junctions.[5] For experiments employing semiconductor/liquid contacts, the redox system in the liquid is not photoexcited but only serves to transport the charge across the interface. This configuration can be used to determine the equilibrium barrier-height of the solid/liquid junction and characterize the

Received: June 21, 2013
Revised: October 8, 2013
Published: January 28, 2014

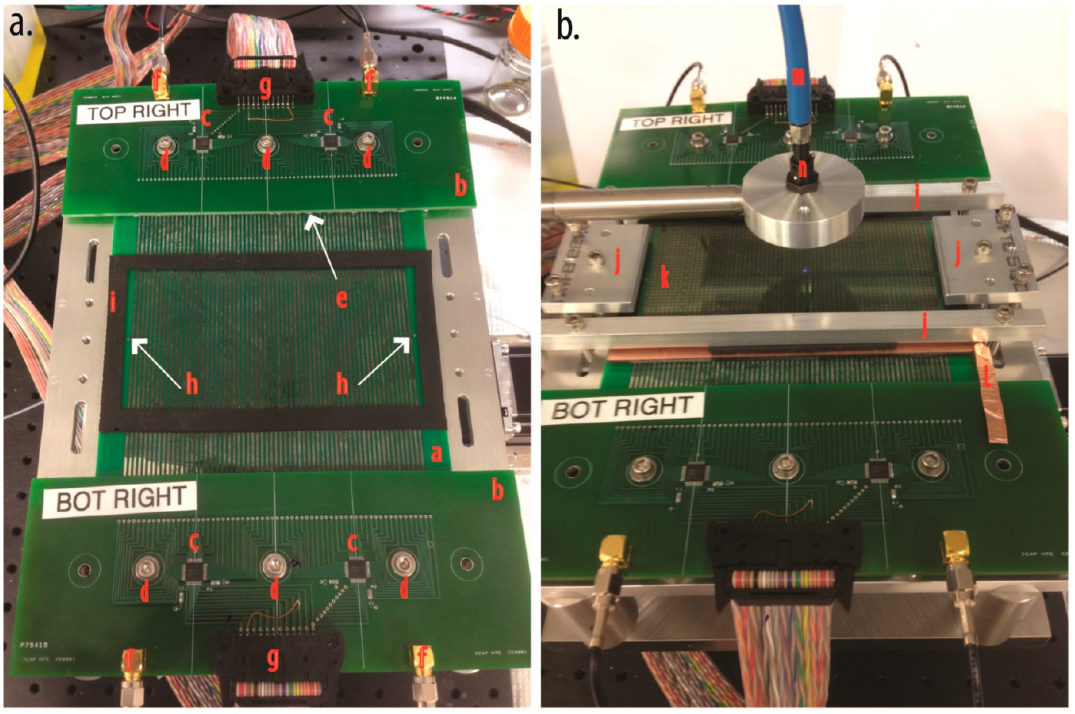

Figure 1. (a) Photograph of the counter electrode assembly in the quantum yield screening system for light absorbers. (b) Photograph of the quantum yield screening system in operation. The individual components labeled in the photos are: (a) the multiplexing counter electrode board, (b) two multiplexer printed circuit boards, (c) four 32-channel multiplexers, (d) mounting holes and screws, (e) silver elastomer connectors, (f) output signal lines, (g) multiplexer control lines, (h) electrolyte solution inlet and outlet ports, (i) 1.6 mm EPDM gasket, (j) four clamps, (k) sample plate containing desired material libraries, (l) electrical connection for working electrode, (m) fiber-coupled LED illumination source, (n) fiber coupled collimator.).

photogeneration, transport and recombination processes in the semiconductor of interest. The resulting energy-conversion properties of such systems are thus directly analogous to those displayed by semiconductor homojunctions or other heterojunctions. High quality semiconductor/liquid contacts have been demonstrated in many material systems, including Si, InP and GaAs,[15−17] with internal quantum yield above 80% for practical applications. While a semiconductor/liquid contact with a reversible redox couple is a very powerful tool for characterizing the properties and performance of photoabsorbers, employing this tool in high throughput screening is challenging. As discussed below, the current pathway for photoelectrochemical redox is easily shunted at by any electrode area beyond the illuminated photoabsorber, especially at short-circuit conditions. Previously reported high throughput devices[6,8,9,12,18−20] are incapable of performing screening with reversible redox couples because of this shunting issue. Another approach is to electrically isolate each sample in the working electrode by photolithography.[7] However, the high cost and long preparation for such substrates are prohibitive for high-throughput material discoveries, prompting our development of a new photoelectrochemical device design.

In this study, we describe a multiplexing counter electrode assembly that is able to deliver fast quantum yield screening and identify the most promising light absorber materials for follow-up studies. We have evaluated the quantum yield of a pseudo-quaternary material system, $(Fe−Zn−Sn−Ti)O_x$, prepared by ink jet printing, with 2112 samples containing 1819 unique compositions and various internal standards. The internal standards are pure metal (Fe, Zn, Sn, and Ti) oxides dispersed throughout the library to monitor any spatial and temporal variations in the measurements performance, which were found to be negligible in this study. Fe_2O_3 is among the most promising and studied metal oxides for photoanodes because of the material abundancy, suitable band energetics, and stability in aqueous electrolytes.[6,19,21] Our exploration of the low-Ti region of the composition space indicates the presence of a new $(Fe−Sn−Ti)O_x$ pseudoternary composition region that exhibits a higher photon-to-electron conversion efficiency than any of the corresponding pseudobinary compositions.

EXPERIMENTAL SECTION

Multiplexing Counter Electrode Assembly. Figure 1 shows photographs of the multiplexing counter electrode assembly. A 15 cm ×15 cm × 2.4 mm counter electrode board (a) and two multiplexer printed circuit boards (b) were designed in PCB Artist and fabricated by Advanced Circuits. Four 32-channel analog multiplexers (c) (ADG732, Analog Device, Inc.) were employed on the two mux boards. Six mounting holes and screws (d) provided mechanical and electrical connection between the multiplexer boards and the counter electrode array via an elastomeric connector (FujiPoly, Silver Zebra) (e). A custom LabVIEW program selected the appropriate multiplexer channel via address and enable lines (g) to route the signal for measurement (f). The 1 mm wide traces on the counter electrode board were augmented with an electroless platinum deposition achieved in a chloroplatinic acid solution. Two 1.6 mm holes (h) were located at the ends of the counter electrode board to serve as the inlet and outlet for the electrolyte solution. A 1.6 mm thick EPDM gasket (i) was cut to fit the 10 cm ×15 cm sample plate and glued onto the

dx.doi.org/10.1021/co400081w | ACS Comb. Sci. 2014, 16, 120−127

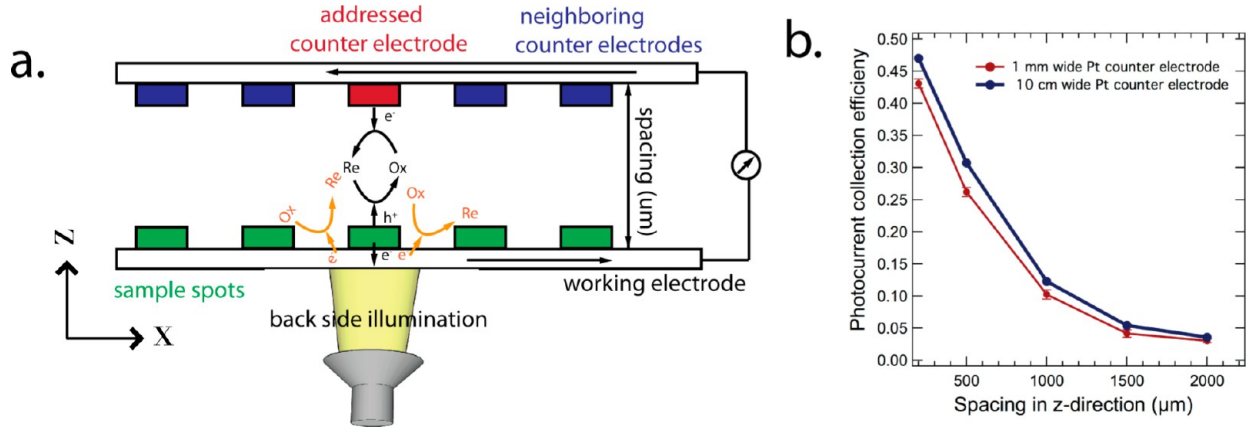

Figure 2. (a) Schematic illustration of the quantum yield screening system where the green rectangles represent the inkjet printed material library and the red rectangle represents the electrically addressed Pt counter electrode and the blue rectangles represent the unaddressed neighboring Pt counter electrodes. The photocurrent shunt pathways that occur at the nearby FTO region are indicated in orange. (b) The fraction of photocurrents collected at the corresponding counter electrode as a function of electrode vertical separation from COMSOL Multiphysics simulations. The red curve shows the result for the center (*x*-direction) Pt counter electrode (1 mm wide) where the sample was underneath the center (*y*-direction) of the counter electrode. The error bars indicate the variations in collection efficiency for the sample spot at different *y*-positions and *x*-positions. The blue curve represents the simulation results for a 10 cm wide center-Pt counter electrode where the sample was directly beneath the center of the counter electrode.

counter electrode board to prevent electrolyte leakage. Four stainless steel clamping bars (j) were used to make a liquid-tight seal around the perimeter of the sample plate (k). The glass sample plate was coated with 400 nm of fluorine-doped tin oxide (FTO) to provide a common conducting surface for all samples (Hartford Glass Company). Adhesive copper tape (l) was used to make electrical contact with the FTO layer. An optical fiber coupled to a 385 nm LED light source (m) and collimating lens (Thorlabs) (n) was positioned above the sample plate and provided a 1.5 mm diameter spot. The optical power delivered to the backside of the sample library was measured to be 50 mW cm^{-2}. The working-to-counter electrode current was synchronized to the switched illumination in the LabVIEW program and was measured with a source meter (Keithley 2400).

Scanning Droplet Photoelectrochemical Cell. The detailed geometry and operational performance of a scanning droplet cell were described by Gregoire, et al.[22] The working principle of the setup used in this study is very similar to many previously reported scanning droplet cells and microcells.[23−26] Briefly, a drop of solution was formed on top of a 1 mm × 1 mm inkjet printed sample. The shape of the droplet was directed and controlled by a solution inlet port and multiple solution outlet ports with no sealing gasket. The scanning droplet cell provided electrical and optical access to the solution drop, including a reference electrode, a counter electrode and a fiber-coupled illumination source. In this study, we used an aqueous 50 mM $[Fe(CN)_6]^{3-/4-}$ redox couple as the feed solution to form a stationary drop contact to the materials of interest. After moving to a new sample location, three short pulses of solution were produced and a few seconds of delay ensured a stable drop contact to the test sample. The solution potential was by a custom-made glass capillary reference electrode containing a platinum wire in the $[Fe(CN)_6]^{3-/4-}$ redox couple. A second platinum wire placed in the solution influent served as the counter electrode. Short-circuit (0 V vs Pt reference electrode) photocurrent measurements were performed with a Gamry G300 potentiostat using chopped, back-side illumination. The 385 nm light source was a high power (100 mW/cm^2), fiber-coupled LED under computer control.

Combinatorial Material Synthesis by Inkjet Printing. The discrete pseudoquaternary (Fe−Zn−Sn−Ti)−O_x library was designed as an array of Fe-rich compositions with approximately 3.33 at% composition steps for each of Fe, Zn, and Sn and 0.33 at% composition steps for Ti. The array of samples was deposited by inkjet printing onto the FTO-coated side of 10 cm ×15 cm glass plate.[22,27] Four separate metal inks of the type previously described by Stuckey group,[28,29] were prepared by mixing 10 mmol of each of the Fe, Zn, and Sn precursors and 1 mmol of the Ti precursor with 0.80 g Pluronic F127 (Aldrich), 1.0 mL glacial acetic acid (T.J. Baker, inc), 0.40 mL of concentrated HNO_3 (EMD), and 30 mL of 200 proof Ethanol (Koptec). The metal precursors were $FeCl_3$ (1.53 g, 97%, Sigma Aldrich), $Zn(NO_3)_2{\cdot}xH_2O$ (2.84 g, 99.99%, Sigma Aldrich, where x = 5 for stoichiometric calculations), $SnCl_2{\cdot}2H_2O$ (2.37 g, ≥98%, Sigma Aldrich), and $Ti(OBu)_4$ (0.34 mL, 97%, Sigma Aldrich). After the library of compositions was printed as a set of 1 mm × 1 mm spots on a 2 mm pitch, the inks were dried and the metal precursors converted to oxides by calcination at 67 °C for 18 h, followed by 5 h at 350 °C in air. Elemental composition analysis was performed on select samples after photoelectrochemical screening using X-ray Fluorescence (EDAX, Orbis). While measurement of Sn concentration in the library was confounded by the FTO layer, the composition measurements showed good agreement with the library design compositions.

Device Simulation. The solution contact to both the multiplexed counter electrode and the common FTO working electrode created complex solution-phase conduction pathways which were modeled to assess the device performance. The photocurrent collection efficiency as a function of the spacing between the planar working electrode and the counter electrode was simulated by solving the 3-D Poisson equation in COMSOL Multiphysics. A periodic boundary condition was employed for the four sidewalls of the simulation region. The Neumann boundary condition for the uniform current flux was applied at the limits of the 1 mm × 1 mm sample. Electrical

dx.doi.org/10.1021/co400081w | ACS Comb. Sci. 2014, 16, 120−127

ground was established at the corresponding counter electrode and the FTO regions around the sample. The conductivity of the electrolyte was set to a value of 10.0 S m^{-1} in the subdomain settings, although this conductivity value is inconsequential for the calculated device performance. A boundary integration was performed both on the FTO area and the corresponding counter electrode to calculate the current flux in these regions.

RESULTS AND DISCUSSION

Operating Principles and Photocurrent Collection Efficiency of the Assembly. The schematic illustration of the multiplexing counter electrode assembly is shown in Figure 2a. The 1 mm × 1 mm inkjet printed material spots (green rectangles) were electrically connected by the underlying FTO layer, which served as a common working electrode during the measurement. The 128 counter electrodes were programmatically addressed using a set of four 32-channel multiplexers. For each photocurrent measurement, the illumination source was aligned with the desired sample and the corresponding Pt counter electrode (red rectangle) was connected to form a closed circuit with the common working electrode. In contact with the $[Fe(CN)_6]^{3-/4-}$ redox couple, the minority carriers (photogenerated holes) were transported to the semiconductor/liquid interface and underwent an oxidation reaction ($[Fe(CN)_6]^{4-} \rightarrow [Fe(CN)_6]^{3-}$). The majority carriers (photoexcited electrons) were collected by the FTO contact and drove the respective reduction reaction ($([Fe(CN)_6]^{3-} \rightarrow [Fe(CN)_6]^{4-}$) either at a neighboring region on the working electrode or at the Pt counter electrode. The latter pathway corresponds to current passing from working to counter electrode, and was measured by the picoammeter. The former pathway, in which electrons were transferred to solution at the working electrode (indicated by orange) acted as a current shunt, resulting in a partial measurement of the photocurrent by the ammeter. We define the photocurrent collection efficiency as the ratio between the measured current (collected at the Pt stripe counter electrode) divided by the total current generated by the sample. The total current generated by the sample was simulated by a Multiphysics model and evaluated by an independent measurement tool, a scanning droplet cell, as described below.

Figure 2b shows the photocurrent collection efficiency as a function of the spacing between the working electrode and the counter electrode from 3-D COMSOL simulations. The two competing pathways for the current collection were dictated by the detailed geometry of the assembly. As the spacing between the working and the counter electrode decreases, the photocurrent collection efficiency increases monotonically. In the Figure 1 device, each counter electrode is paired with a column of 16 or 17 samples along the y-direction. The simulation results indicated that the photocurrent collection efficiency for this set of y-positions varies by approximately 2%, which is negligible for high throughput screening. In this study, we used a 1.6 mm EPDM gasket as the spacer between the two electrodes. After application of the clamps (Figure 1), the spacing was reduced to about 1.3 mm. This spacing corresponds to a collection efficiency of approximately 7.5%. A higher collection efficiency, ε, can be readily attained by either decreasing the electrode separation z or increasing the area of the active counter electrode. Should the former strategy be adopted, care must be taken to ensure the spacing is uniform over the sample library, as any nonuniformity, Δz, will introduce a systematic error of magnitude $\Delta z\ d\varepsilon/dz$, where $d\varepsilon/dz$ is the slope of the curve in Figure 2b and rapidly increases at low electrode separation. As shown in Figure 2b, the collection efficiency can also be increased by employing a larger area counter electrode. However, the simulation results indicated that the collection efficiency increased by less than 5% when the width of the counter electrode stripe increased by 2 orders of magnitude. In addition, this approach has two adverse effects on the experiment, most directly in that the larger counter electrode will result in both increased magnitude and increased fluctuations in the background or "dark" current. The fluctuations in the dark current, which may vary significantly for different composition libraries, impact the sensitivity of the photocurrent measurement. The other adverse effect of increasing the counter electrode area is that it eliminates the capability of performing parallel measurements, as discussed below.

Quantum Yield Screening of a Quaternary Material Library. Figure 3a shows three representative photocurrent measurements as a function of time from the (Fe−Zn−Sn−Ti)O_x material library in contact with a 50 mM $[Fe(CN)_6]^{3-/4-}$ redox couple. During the measurements, each sample spot was exposed to a chopped illumination source (50 mW cm^{-2} at 385 nm) with a 1 Hz frequency incident from the back. Short-circuit photocurrents were measured between the common working electrode and the corresponding Pt stripe counter electrode. A consequence of multiplexing is a reduction in the counter electrode area, which resulted in dark currents well

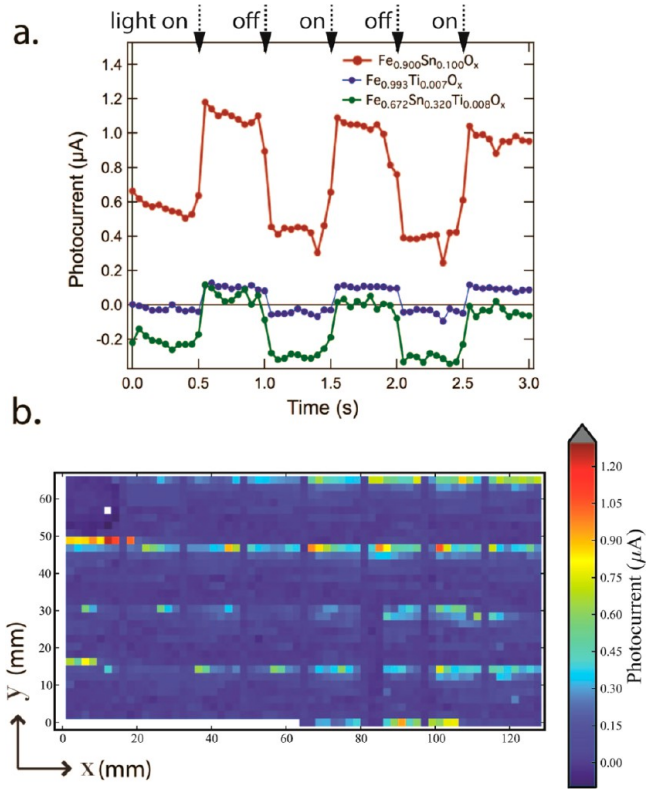

Figure 3. (a) Three representative short-circuit current measurements from the (Fe−Zn−Sn−Ti)O_x sample plate in contact with a 50 mM $[Fe(CN)_6]^{3-/4-}$ redox couple under a chopped (1 Hz) illumination at 385 nm. (b) Photocurrent values for 2112 (1819 test and 293 reference) samples from the (Fe−Zn−Sn−Ti)O_x material library that was inkjet printed on an FTO-coated glass plate.

dx.doi.org/10.1021/co400081w | ACS Comb. Sci. 2014, 16, 120−127

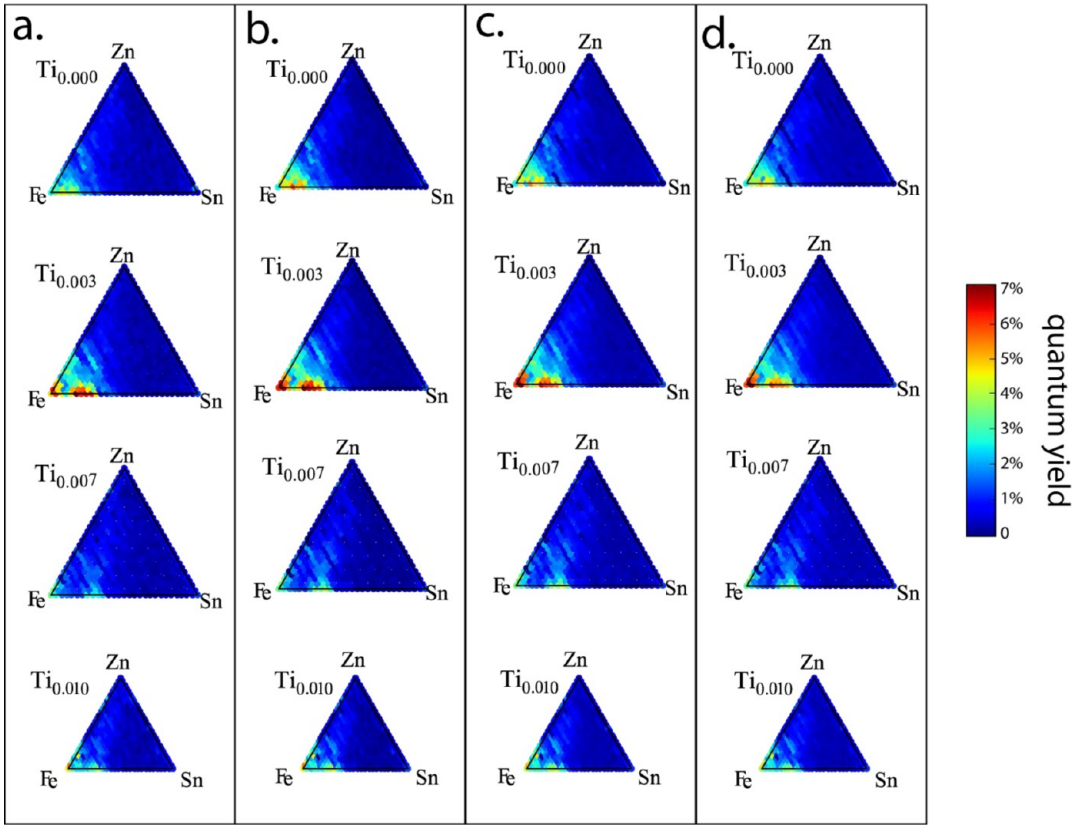

Figure 4. Short-circuit photocurrent values of material compositions in the (Fe−Zn−Sn−Ti)O_x quaternary library plotted as pseudoternary ternary slices separated by 0.33 at.% intervals of Ti concentration. The 4 columns of plots (a, b, c, d) correspond to repeated screenings of the library with different starting points and scan directions.

below 1 μA and measurable photocurrent values as low as 100 nA (corresponding to 10 μA cm^{-2}). The calculated 7.5% photocurrent collection efficiency of the instrument, which is in excellent agreement with the scanning droplet cell measurement described below, must be considered to relate this photocurrent detection limit to that of the photoabsorber's external quantum yield. For the 385 nm, 50 mW cm^{-2} illumination source used in the present study, the detection limit of external quantum yield is 0.5%. By coupling the fiber optic in Figure 1 to an AM1.5 light source, solar external quantum yield measurements can be made with a detection limit of 0.3%.

Figure 3b shows the photocurrent values of 1819 unique material compositions from the (Fe−Zn−Sn−Ti)O_x library. Analysis of the photocurrent values showed no correlation with the physical location of the sample in the library, and as discussed below, the photocurrent screen revealed important trends with respect to sample composition. Figure 4 shows the external quantum yield map from four independent photocurrent screening results of the (Fe−Zn−Sn−Ti)O_x library. In the physical plate as shown in Figure 3b, four different scanning directions were employed: rastering along x from the upper right corner (a), rastering along y from the upper right corner (b), rastering along x from the bottom right corner (c) and rastering along y from the bottom right corner (d). The resulting data was plotted as pseudoternary ternary slices separated by 0.33 at.% intervals of Ti concentration. The four different screenings showed excellent agreement with an average variation in photocurrent of less than 5% between any pair of experiments. In Figure 4 the quaternary composition space is visualized as a series of pseudoternary $(Fe−Zn−Sn)_{1-y}Ti_yO_x$ spaces with Ti atomic concentrations, y = 0 at.%, 0.033 at.%, 0.067 at.% and 0.1 at.%. In the y = 0.033 at.% plane, an interesting nonmonotonic trend along the Fe−Sn boundary is observed with optimal Fe:Sn ratio close to 8.5:1. The pseudoternary plots with neighboring Ti concentrations show similar trends, demonstrating that the ternary (Fe−Sn−Ti)O_x region contains the highest performing photoabsorbers in the library. The global maximum of external quantum yield is approximately 7% with nominal printed composition of $Fe_{0.894}Sn_{0.103}Ti_{0.0034}O_x$. This composition region exhibited higher photocurrents compared to the pure metal oxides and any binary metal oxide in the array. Incorporating either Sn^{4+} or Ti^{4+} into Fe_2O_3 as a binary system has been reported to show improved anodic photoelectrochemical performance by several research groups.[6,19,30−32] In most cases, the enhancement of the performance has been attributed to the improvement of the conductivity due to the increase in donor density.[6,19,30−32] However, the ternary material space, (Fe−Sn−Ti)O_x, has not been previously investigated. Further studies including the crystalline phases, surface structures, optical absorption spectra and band energetics of the "hit" material compositions are needed to elucidate the underlying mechanism for enhanced quantum yield measurements observed in this study. The absolute quantum yield value even with the same material composition varies in the literature depending on the synthesis techniques, for example, the Bard group reported the binary (Fe−Sn)O_x system with quantum yields below 5%[6,19] while Uchiyama et. al,[30] observed a significantly higher quantum yield (>20%) in the same material system. The photocurrent-

dx.doi.org/10.1021/co400081w | ACS Comb. Sci. 2014, 16, 120−127

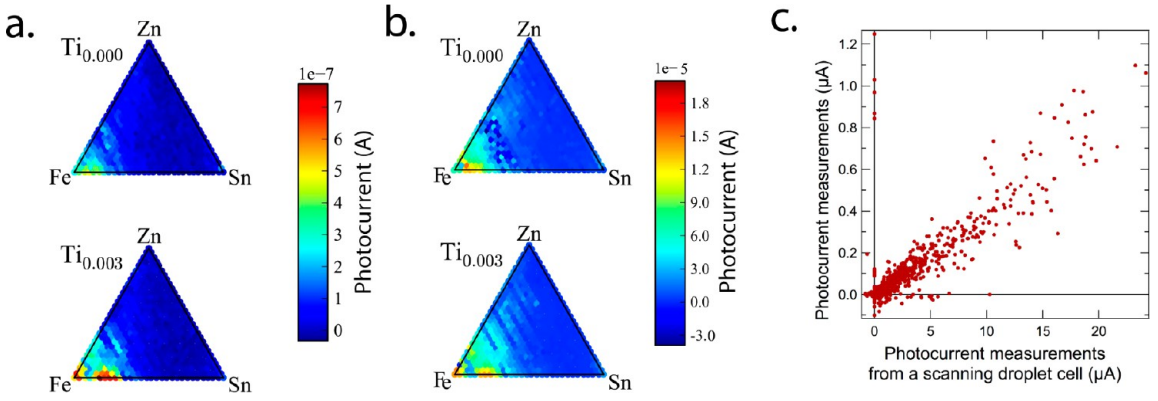

Figure 5. (a) Ternary compositional slices of the short-circuit photocurrent measurements from the multiplexing counter electrode with a thin layer assembly. (b) Ternary compositional slices of the short-circuit photocurrent measurements from a scanning droplet cell. (c) Comparison of photocurrent measurements from both screening techniques for the corresponding samples shown in panels a and b.

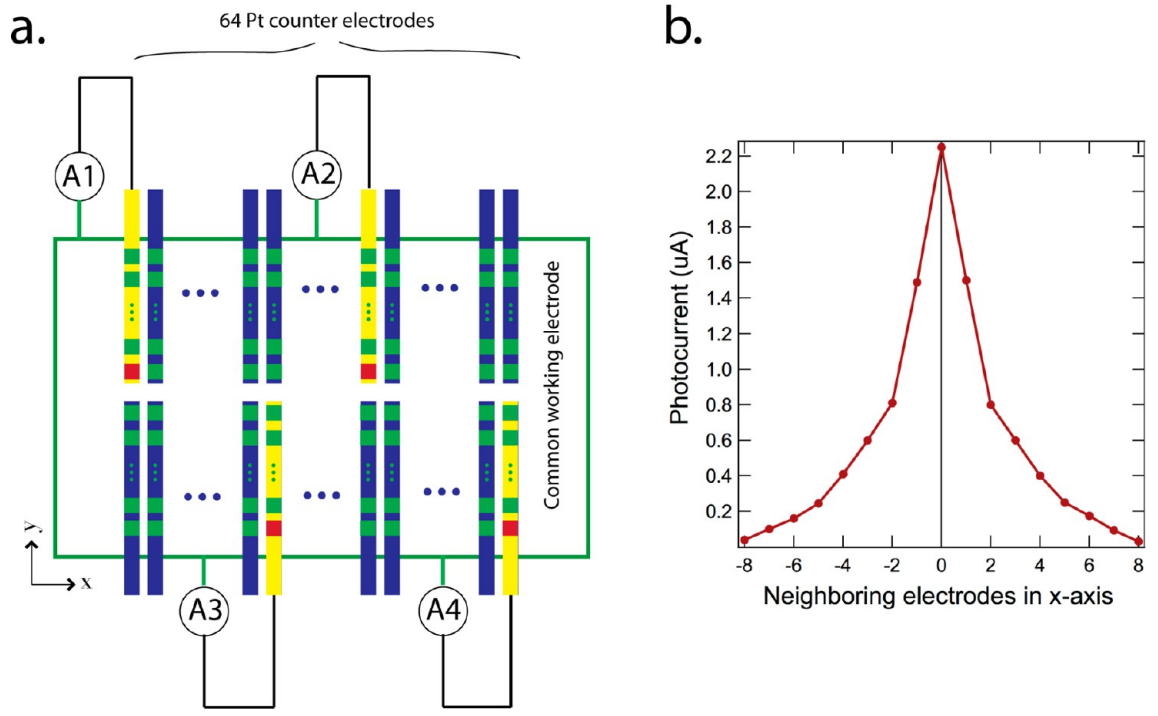

Figure 6. (a) Schematic illustration of a 4-fold parallel photocurrent measurement. The red squares represent samples under illumination and the green squares represent samples in the dark. The yellow rectangles represent the addressed four Pt counter electrodes, while the blue rectangles represent the rest unaddressed Pt counter electrodes. (b) Crossover photocurrent measured at the neighboring electrodes when a sample at the middle electrode (0-electrode) was under illumination.

composition trends in this study indicate the utility of multielement alloying for improvement of Fe_2O_3-based photoabsorbers.

Screening Validation and the Quantum Yield Calibration Factor. Independent short-circuit photocurrent measurements on the (Fe−Zn−Sn−Ti)O_x library were carried out using a scanning droplet photoelectrochemical cell in which solution contact was made to each sample individually to perform a 3-electrode electrochemical experiment. Figure 5a and 5b show the photocurrent map from the multiplexing counter electrode assembly and the scanning droplet measurements respectively. The two screening methods yielded the same photocurrent trend and identified the global maximum at the same composition region. The sample by sample correlation from the two experiments is shown in Figure 5c, where the abscissa represents the photocurrent values from the scanning droplet cell and the ordinate corresponds to the photocurrent values from the multiplexed counter electrode assembly. Considering the output illumination power from both measurements and the photocurrent collection efficiency simulated in Figure 1b at 1.3 mm vertical separation, a photocurrent ratio between the two measurements of 0.0375 was expected. The slope of the linear least-squares regression fit of the data in Figure 5c was determined to be 0.038, which is in excellent agreement with the calculated value. The calculated and experimentally verified slope can be utilized as a calibration factor to correct the shunting behavior of the multiplexed counter electrode assembly, yielding the full external quantum yield of each sample.

dx.doi.org/10.1021/co400081w | ACS Comb. Sci. 2014, 16, 120−127

Sample Throughput and Parallel Measurements. To demonstrate the performance of the multiplexed photocurrent measurement device, the experiments presented in this manuscript were performed at high but not optimal throughput. Specifically, data from three illumination cycles were collected in which a relatively low illumination chopping frequency of 1 Hz was used. For attaining higher throughput in serial screening mode, a 0.1s dark current measurement followed by a single 0.1 s illumination pulse (i.e., 5 Hz) has been used to screen a wide variety of materials, yielding a throughput of approximately 1 s per sample. The chopping frequency may be practically limited by the photocurrent equilibration time scale after a step function illumination, which is dependent on the sample composition and structure. The electrochemical double layer charging time scale may also limit this frequency, especially for porous materials.

The multiplexed counter electrode design affords the ability to perform parallel photocurrent measurements as a result of the small area of each counter electrode relative to the large-area common working electrode. The counter electrode geometry shown in Figure 1 provides an excellent compromise between current collection efficiency and ability for parallel measurements. The high aspect ratio counter electrode provides current collection efficiency along its long axis and spatially resolved collection along its short axis. It is along the narrow direction that parallel measurements can be performed by using multiple light sources to illuminate a set of samples. While each sample shares the common working electrode, connecting each counter electrode to an individual picoammeter provides sample-resolved photocurrent measurements. A schematic for the 4-fold measurement of photocurrent is shown in Figure 6a.

The primary concern for operating in this parallel measurement mode is the current crosstalk that is facilitated by conduction through the electrolyte. The crosstalk behavior between the active sample and its neighboring counter electrodes (blue rectangles in Figure 1a) was measured by illuminating the active sample and performing sequential photocurrent measurements at each neighboring counter electrode. Figure 6b shows that the crosstalk photocurrents between the neighboring electrodes decrease significantly as the distance between the sample and the addressed counter electrode increases. Beyond the eight nearest neighbor electrodes, the crosstalk photocurrent decreased to less than 3% of the central photocurrent. Thus, parallel photocurrent measurements can be confidently performed simultaneously if the active samples are more than 16 electrodes (32 mm) away. The instrument described in this manuscript contains four multiplexers (see Figure 1), which enables 4-fold parallel measurements (see Figure 6a) and a corresponding increase in experiment throughput. With the presented sample geometry, 10-fold parallel measurements could be implemented. Higher order parallel measurements are enabled by either decreasing the electrode spacing z (see Figure 1b) or altering the sample library layout. It is worth noting that for the serial measurements presented in this manuscript, there is no crosstalk because of the use of a single multiplexed counter electrode and single illumination source.

It is worth noting that the most pertinent features of this instrument design for high throughput studies are the common working electrode and continuous electrolyte solution contact. Synthesis of composition libraries with addressable working electrode contacts is prohibitively expensive and establishing individual solution contact to each sample in a library is time-consuming. The device design presented in this manuscript essentially allows parallel, simultaneous preparation of thousands of photoelectrochemical cells. The experiment preparation throughput is thus enhanced by a factor of several thousand compared to traditional techniques.

CONCLUSIONS

A photoelectrochemical cell with carefully designed geometry was developed to perform high throughput photoabsorber screening on a sample library with shared electrical contact and electrolyte solution. The multiplexing counter electrode assembly described herein demonstrated a photocurrent sensitivity of sub-10 μA cm^{-2} with an external quantum yield sensitivity of 0.5% for a thin film sample under a LED illumination source (385 nm, 50 mW cm^{-2}). The external quantum yield of 1819 samples from a pseudoquaternary metal oxide library, (Fe−Zn−Sn−Ti)O_x, were screened with a sample throughput of 3.3 s per sample and the capability for throughput of 1 s per sample has been demonstrated in serial scanning mode. Further increases in throughput can be attained by exploiting the multiplexed counter electrode assembly to perform simultaneous parallel measurements. Independent measurements from a series of photocurrent measurements in which a solution droplet contact was made to each sample showed a strong correlation with the screening results from the multiplexing counter electrode assembly. Preliminary screen results indicated a promising ternary composition near $Fe_{0.894}Sn_{0.103}Ti_{0.0034}O_x$, that has a quantum yield of 6.7% at 385 nm, greater than that of any associated binary composition. Decreasing the separation between the working electrode and the counter electrode can further increase the current collection efficiency and improve the photocurrent sensitivity. For parallel measurements, the decreased spacing also decreases the crosstalk between the neighboring electrodes, which can in turn improve the measurement resolution and enable higher order parallel measurements.

AUTHOR INFORMATION

Corresponding Authors

*E-mail: cxx@caltech.edu.

*E-mail: gregoire@caltech.edu.

Notes

The authors declare no competing financial interest.

ACKNOWLEDGMENTS

This material is based upon work performed by the Joint Center for Artificial Photosynthesis, a DOE Energy Innovation Hub, supported through the Office of Science of the U.S. Department of Energy under Award Number DE-SC000499. We gratefully acknowledge critical support and infrastructure provided for this work by the Kavli Nanoscience Institute at Caltech.

REFERENCES

(1) Walter, M. G.; Warren, E. L.; McKone, J. R.; Boettcher, S. W.; Mi, Q. X.; Santori, E. A.; Lewis, N. S. Solar Water Splitting Cells. *Chem. Rev.* **2010**, *110* (11), 6446−6473.

(2) Sze, S. M. *Physics of Semiconductor Devices*, 3rd ed.; John Wiley and Sons: New York, 1981.

(3) Lewis, N. S.; Nocera, D. G. Powering the Planet: Chemical Challenges in Solar Energy Utilization. *Proc. Natl. Acad. Sci. U.S.A.* **2006**, *103* (43), 15729−15735.

(4) Sailor, M. J.; Klavetter, F. L.; Grubbs, R. H.; Lewis, N. S. Electronic-Properties of Junctions between Silicon and Organic Conducting Polymers. *Nature* **1990**, *346* (6280), 155−157.
(5) Lewis, N. S. A Quantitative Investigation of the Open-Circuit Photovoltage of the Semiconductor Liquid Interface. *J. Electrochem. Soc.* **1984**, *131* (11), 2496−2503.
(6) Jang, J. S.; Lee, J.; Ye, H.; Fan, F. R. F.; Bard, A. J. Rapid Screening of Effective Dopants for Fe_2O_3 Photocatalysts with Scanning Electrochemical Microscopy and Investigation of Their Photoelectrochemical Properties. *J. Phys. Chem. C* **2009**, *113* (16), 6719−6724.
(7) Katz, J. E.; Gingrich, T. R.; Santori, E. A.; Lewis, N. S. Combinatorial Synthesis and High-Throughput Photopotential and Photocurrent Screening of Mixed-Metal Oxides for Photoelectrochemical Water Splitting. *Energy Environmental Science* **2009**, *2* (1), 103−112.
(8) Woodhouse, M.; Herman, G. S.; Parkinson, B. A. Combinatorial Approach to Identification of Catalysts for the Photoelectrolysis of Water. *Chem. Mater.* **2005**, *17* (17), 4318−4324.
(9) Woodhouse, M.; Parkinson, B. A. Combinatorial Approaches for the Identification and Optimization of Oxide Semiconductors for Efficient Solar Photoelectrolysis. *Chem. Soc. Rev.* **2009**, *38* (1), 197−210.
(10) Jaramillo, T. F.; Baeck, S. H.; Kleiman-Shwarsctein, A.; Choi, K. S.; Stucky, G. D.; McFarland, E. W. Automated Electrochemical Synthesis and Photoelectrochemical Characterization of Zn1−*x*CoxO Thin Films for Solar Hydrogen Production. *J. Comb. Chem.* **2005**, *7* (2), 264−271.
(11) Park, H. S.; Kweon, K. E.; Ye, H.; Paek, E.; Hwang, G. S.; Bard, A. J. Factors in the Metal Doping of BiVO4 for Improved Photoelectrocatalytic Activity as Studied by Scanning Electrochemical Microscopy and First-Principles Density-Functional Calculation. *J. Phys. Chem. C* **2011**, *115* (36), 17870−17879.
(12) Ye, H.; Lee, J.; Jang, J. S.; Bard, A. J. Rapid Screening of $BiVO_4$-Based Photocatalysts by Scanning Electrochemical Microscopy (SECM) and Studies of Their Photoelectrochemical Properties. *J. Phys. Chem. C* **2010**, *114* (31), 13322−13328.
(13) Olsen, L. C.; Addis, F. W.; Miller, W. Experimental and Theoretical-Studies of Cu_2O Solar-Cells. *Sol. Cells* **1982**, *7* (3), 247−279.
(14) Wang, F. C.; Fahrenbruch, A. L.; Bube, R. H. Transport Mechanisms for Mg/Zn3p2 Junctions. *J. Appl. Phys.* **1982**, *53* (12), 8874−8879.
(15) Gronet, C. M.; Lewis, N. S. Design of a 13-Percent Efficient N-Gaas1-Xpx Semiconductor-Liquid Junction Solar-Cell. *Nature* **1982**, *300* (5894), 733−735.
(16) Gronet, C. M.; Lewis, N. S.; Cogan, G.; Gibbons, J. N-Type Silicon Photoelectrochemistry in Methanol—Design of a 10.1-Percent Efficient Semiconductor Liquid Junction Solar-Cell. *Proc. Natl. Acad. Sci. U. S. A.* **1983**, *80* (4), 1152−1156.
(17) Heben, M. J.; Kumar, A.; Zheng, C.; Lewis, N. S. Efficient Photovoltaic Devices for Inp Semiconductor Liquid Junctions. *Nature* **1989**, *340* (6235), 621−623.
(18) Lee, J.; Ye, H.; Pan, S.; Bard, A. J. Screening of Photocatalysts by Scanning Electrochemical Microscopy. *Anal. Chem.* **2008**, *80* (19), 7445−50.
(19) Jang, J. S.; Yoon, K. Y.; Xiao, X. Y.; Fan, F. R. F.; Bard, A. J. Development of a Potential Fe_2O_3-Based Photocatalyst Thin Film for Water Oxidation by Scanning Electrochemical Microscopy: Effects of Ag-Fe_2O_3 Nanocomposite and Sn Doping. *Chem. Mater.* **2009**, *21* (20), 4803−4810.
(20) Ye, H.; Park, H. S.; Bard, A. J. Screening of Electrocatalysts for Photoelectrochemical Water Oxidation on W-Doped $BiVO_4$ Photocatalysts by Scanning Electrochemical Microscopy. *J. Phys. Chem. C* **2011**, *115* (25), 12464−12470.
(21) Sivula, K.; Le Formal, F.; Gratzel, M. Solar Water Splitting: Progress Using Hematite (α-Fe_2O_3) Photoelectrodes. *ChemSusChem* **2011**, *4* (4), 432−449.
(22) Gregoire, J. M.; Xiang, C. X.; Liu, X. N.; Marcin, M.; Jin, J. Scanning Droplet Cell for High Throughput Electrochemical and Photoelectrochemical Measurements. *Rev. Sci. Instrum.* **2013**, *84*, No. 024102.
(23) Hassel, A. W.; Lohrengel, M. M. The Scanning Droplet Cell and Its Application to Structured Nanometer Oxide Films on Aluminium. *Electrochim. Acta* **1997**, *42* (20−22), 3327−3333.
(24) Schafer, D.; Mardare, C. C.; Savan, A.; Sanchez, M. D.; Mei, B.; Xia, W.; Muhler, M.; Ludwig, A.; Schuhmann, W. High-Throughput Characterization of Pt Supported on Thin Film Oxide Material Libraries Applied in the Oxygen Reduction Reaction. *Anal. Chem.* **2011**, *83* (6), 1916−1923.
(25) Schultze, J. W.; Bressel, A. Principles of Electrochemical Micro- and Nano-System Technologies. *Electrochim. Acta* **2001**, *47* (1−2), 3−21.
(26) Schultze, J. W.; Tsakova, V. Electrochemical Microsystem Technologies: From Fundamental Research to Technical Systems. *Electrochim. Acta* **1999**, *44* (21−22), 3605−3627.
(27) Gregoire, J. M.; Xiang, C.; Mitrovic, S.; Liu, X.; Marcin, M.; Cornell, E. W.; Fan, J.; Jin, J. Combined Catalysis and Optical Screening for High Throughput Discovery of Solar Fuels Catalysts. *J. Electrochem. Soc.* **2013**, *160* (4), F337−F342.
(28) Fan, J.; Boettcher, S. W.; Stucky, G. D. Nanoparticle Assembly of Ordered Multicomponent Mesostructured Metal Oxides via a Versatile Sol−Gel Process. *Chem. Mater.* **2006**, *18* (26), 6391−6396.
(29) Liu, X. N.; Shen, Y.; Yang, R. T.; Zou, S. H.; Ji, X. L.; Shi, L.; Zhang, Y. C.; Liu, D. Y.; Xiao, L. P.; Zheng, X. M.; Li, S.; Fan, J.; Stucky, G. D. Inkjet Printing Assisted Synthesis of Multicomponent Mesoporous Metal Oxides for Ultrafast Catalyst Exploration. *Nano Lett.* **2012**, *12* (11), 5733−5739.
(30) Uchiyama, H.; Yukizawa, M.; Kozuka, H. Photoelectrochemical Properties of Fe_2O_3−SnO_2 Films Prepared by Sol−Gel Method. *J. Phys. Chem. C* **2011**, *115* (14), 7050−7055.
(31) Frydrych, J.; Machala, L.; Tucek, J.; Siskova, K.; Filip, J.; Pechousek, J.; Safarova, K.; Vondracek, M.; Seo, J. H.; Schneeweiss, O.; Gratzel, M.; Sivula, K.; Zboril, R. Facile Fabrication of Tin-Doped Hematite Photoelectrodes—Effect of Doping on Magnetic Properties and Performance for Light-Induced Water Splitting. *J. Mater. Chem.* **2012**, *22* (43), 23232−23239.
(32) Aroutiounian, V. M.; Arakelyan, V. M.; Shahnazaryan, G. E.; Hovhannisyan, H. R.; Wang, H. L.; Turner, J. A. Photoelectrochemistry of Tin-Doped Iron Oxide Electrodes. *Solar Energy* **2007**, *81* (11), 1369−1376.